A Controllably Adhesive Climbing Robot Using Magnetorheological Fluid

Nicholas Wiltsie
Robotic Mobility Group
Massachusetts Institute of Technology
Cambridge, MA 02193
Email: nwiltsie@mit.edu

Michele Lanzetta
University of Pisa
Pisa, Italy
Email: lanzetta@unipi.it

Karl Iagnemma
Robotic Mobility Group
Massachusetts Institute of Technology
Cambridge, MA 02193
Email: kdi@mit.edu

***Abstract*—The novel adhesive effects of magnetorheological fluid for use in climbing robotics were experimentally measured and compared to existing derived models. Contrary to these models, the fluid thickness between two parallel plates was found to have little effect on the adhesive failure strength and a positive effect on time to failure. Target surface roughness was found to have a detrimental effect on pull-off adhesion and a positive effect for shearing loads. A robot capable of adhering to ceilings was designed and shown to be capable of holding 7.6 kPa of adhesive stress in both shear on rough vertical surfaces and normal force on glass sheets, demonstrating a novel form of adhesion on a wide range of surface roughnesses and orientations.**

I. INTRODUCTION

Various methods have been developed for achieving locomotion on inclined, vertical, and inverted surfaces. One of the simplest solutions for adhesion involves pressure-sensitive adhesives (PSAs) such as tape [1]. PSAs use a compliant layer of material to conform to the target surface, maximizing the contact area and creating adhesion through van der Waals forces. As van der Waals forces scale as $1/h^3$, where h is the local separation between the material and substrate, the surfaces typically must lie within a few hundreds of nanometers of each other. PSAs can be designed to exhibit high adhesive forces but can often require relatively high forces for attachment and detachment and are subject to rapid fouling by dust and dirt.

A non-adhesive approach to enable climbing on vertical surfaces is based on the engagement of small spikes ("microspines") with surface asperities [2][3]. While not true adhesion, this approach enables "clinging" to surfaces with high degrees of roughness, such as stucco and brick. This technology generally cannot be employed on smooth surfaces, and can potentially damage a flexible substrate; additionally, microspines can be subject to plastic deformation and wear even under moderate loading due to the high Hertzian contact stresses at the sharp spike tips.

Recently, adhesive locomotion has been achieved through the use of bio-inspired materials. Gecko lizards can achieve impressive climbing performance through the ability of their appendages to adhere to a wide variety of surfaces [4]. These appendages exhibit hierarchically compliant microstructures which allow them to conform to rough and undulating surfaces over multiple length scales and achieve intimate contact. This van der Waals forces induced by such intimate contact produce sufficient adhesion for climbing. Moreover, gecko adhesive forces also exhibit directionality, allowing the gecko to adhere to surfaces with small preload forces in the normal direction and to detach with small pull-off force. However, the synthetic Gecko-like adhesives that have been developed to date are subject to fouling (like PSAs), are only effective on glass and other smooth surfaces, and are difficult to manufacture [5].

Various dry adhesives have been developed, including those based on arrays of multi-wall carbon nanotubes [6][7] and polymer fibers [8][9]. These adhesives can achieve moderate levels of adhesion only with careful surface preparation and high normal preloads. Also, the size and shape of the contacting elements is important in sustaining adhesion [10][11]. For extremely small elements such as carbon nanotubes, shape sensitivity is low, but for softer materials and larger features on the order of 100 μm the contacting element geometry dramatically affects adhesion.

The use of magnets and magnetic running gear, such as magnetic wheels and track shoes is another common way of achieving adhesion [12][13]. Such approaches have the obvious drawback of being effective only on ferrous substrates. Devices employing electrostatic forces have recently been developed in the context of climbing robotic systems, and have been shown to be effective on a wide variety of surface types [14][15].

The novel form of controllable adhesion based on magnetorheological fluid explored in this paper is unique in that it can potentially be applied to a wide range of surface conditions (i.e. substrate types and roughnesses) and yield large clamping pressures without needing a ferrous substrate. This approach could potentially overcome problems with dust and other surface contaminants. One potential drawback is that fluid may be deposited on the substrate, potentially leaving evidence of the locomotion device's presence or staining the substrate with oil. Preliminary research has shown, however, that it may be possible to recover most of the active fluid that is deposited during the adhesion process.

II. BACKGROUND

Magnetorheological fluids (MRFs) are "active" or "smart" fluids composed of micrometer-scale iron particles suspended in an inert oil. Under an applied magnetic field, these iron particles form a microstructure that dramatically increases

the viscosity of the MRF. Under sufficient fields this microstructure changes the fluid into a Bingham plastic, also known as a yield-stress fluid, that can sustain finite stresses without flowing. This effect disappears when the applied field is removed.

As observed by Ewoldt *et al.* [16], ordinary Newtonian fluids can exhibit a dynamic adhesive force when spread in a thin layer between two parallel plates in a phenomenon known as Stefan adhesion. Neglecting capillary effects and line traction, the adhesive force generated by cylindrical drop of fluid with radius R is given by the integral of the fluid gage pressure field, p:

$$F_{adhesion} = -2\pi \int_0^R p(r) r dr \tag{1}$$

As the two plates are separated, the incompressible fluid is driven toward the center by a negative pressure gradient; this pressure gradient that can dip beneath the ambient pressure, resisting the separation and acting as an adhesive force. For Newtonian fluids, this effect is dependent upon the relative motion of the plates; with no motion, there is no pressure gradient, limiting this effect to dynamic conditions.

By contrast, yield stress fluids can sustain static adhesive and shear forces. For brevity's sake a partial derivation is shown here; however, a full discussion can be found in [16].

Ewoldt *et al.* characterized the LORD MRF-132DG [17] used in this study as increasing in yield stress with the square of the applied field:

$$\sigma_y = \sigma_{y0} + \alpha B^2, \tag{2}$$

where σ_{y0} is the small no-field yield stress and B is the magnetic field strength in teslas. For these experiments the parameters were measured to be $\sigma_{y0} \approx 6.24$ Pa and $\alpha = 137737$ Pa/T^2.

With this known yield stress, the adhesive strength of the fluid with radius R and thickness h exposed to a homogenous magnetic field strength B can be found to be:

$$F_{MRF} = \frac{2}{3}(\sigma_{y0} + \alpha B^2)\pi R^2 \left(\frac{R}{h}\right). \tag{3}$$

Equation 3 is factored to emphasize the effect of the yield stress, σ_y, acting on an area πR^2 in a thin gap, $(R/h) \gg 1$.

If the fluid radius exceeds that of the magnet (R_m), it is exposed to non-homogenous field intensities. Again omitting the derivation, the adhesive force for this situation can be found to be

$$\frac{F_{MRF}}{F_m} = 2 - \left(\frac{R}{R_m}\right)^{-3} + \frac{\sigma_{y0}}{\alpha B_0^2}\left(\frac{R}{R_m}\right)^3 (R > R_m) \tag{4}$$

where $F_m = \frac{2}{3}\pi\alpha B_0^2 R_m^3/h_0$ and B_0 is the homogenous field strength beneath the magnet.

The static shearing force that a yield stress fluid can bear is found as the simple multiplication of the yield stress by the active area:

$$F_{MRF,shear} = (\sigma_{y0} + \alpha B^2)\pi R^2. \tag{5}$$

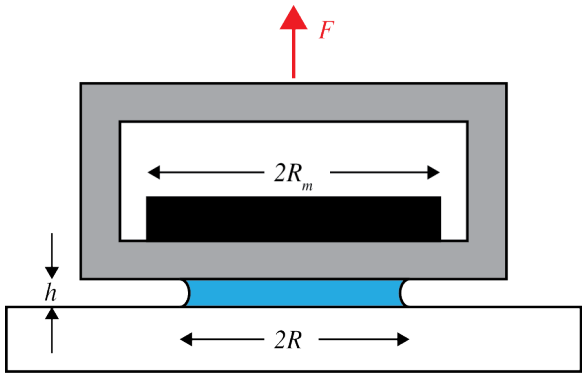

Fig. 1. Graphic of the experimental design. A volume of MRF is placed on the test surface and squeezed into a cylinder of height h and radius R by an open-ended acrylic cube. A magnet with radius $R_m > R$ (shown in black) is placed inside this cube directly above the MRF.

III. EXPERIMENTAL DESIGN

A. Equipment

In order to experimentally verify the effect of fluid thickness h on the adhesive force, shown in Equation 3, a TA.XTplus Texture Analyzer was used to perform tensile loading tests on a sample of MRF [17]. The Texture Analyzer is a linear load/displacement machine capable of applying specified strain rates or sustained loads to a test sample and recording the resultant force and displacement. A 50 mm diameter by 12 mm thick neodymium disk magnet was used as the magnetic field source.

The bottom plate of the testing assembly was attached with four bolts to a TA-90 heavy duty TA.XT2 accessory platform in order to allow a camera to fit underneath the test sample. Acrylic, rolled aluminum, lightly knurled aluminum, teflon, glass, and 110 grit sandpaper bonded to acrylic were used as varying textures for the bottom plate. As shown in Figure 1, a hollow acrylic cube with open sides was attached to a 5 kg load cell and used for the top plate. This cube design to allow the magnet to be placed and removed without changing the plate height. The average magnetic flux generated by the permanent magnet through the top plate was measured as 0.20 T across the face of the magnet by an F.W. Bell 5180 Gauss/Tesla meter.

A pipette was used to deposit a small volume of MRF between the two parallel top and bottom plates. The pipette was on weighed on a Mettler Toledo XS64 analytical balance before and after fluid deposition in order to determine the mass of the MRF sample. The height of the top plate was manually reduced until the MRF contact patch reached a diameter of 24 mm, as measured with a ruler through the top plate. As the testing machine and load cell exhibited complainant behavior, the fluid thickness at this point was determined by combining the measured area and mass with the average fluid density of 3.0 g/cm^3 given by the data sheet [17]. An experimental diameter of 24 mm was determined to be sufficient to overcome edge effects from surface tension while experiencing a homogenous field from the magnet.

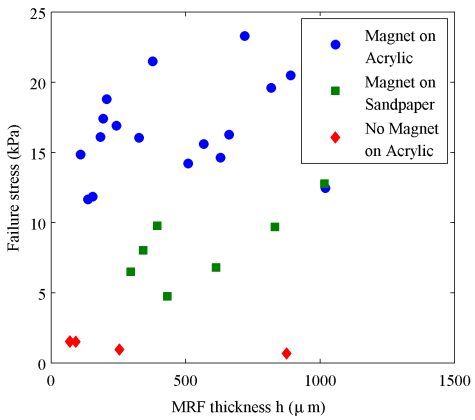

Fig. 2. Peak adhesive forces for 24mm diameter MRF samples. The average flux was measured to be 0.2 T.

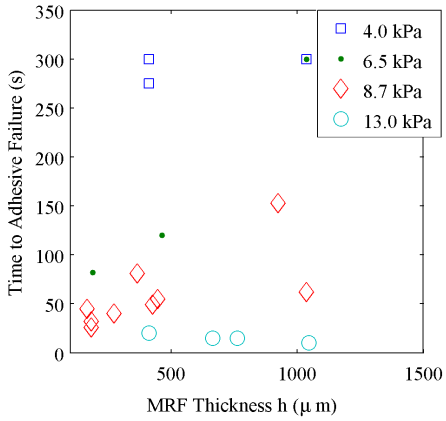

Fig. 3. A plot of the time to failure of various 24 mm diameter MRF samples subjected to different normal stress levels.

B. Failure Stress

Once the fluid sample was prepared as detailed in Section III-A, the magnet was optionally placed in the top plate to activate the fluid. The testing machine raised the top plate at a rate of 10 μm/s (the slowest speed available) and recorded the resulting adhesive force on the top plate at 200 Hz for the duration of the experiment. Each trial lasted until the MRF failed, as seen by a drastic reduction in probe force or by a visual separation of the two plates. The plates were cleaned and the fluid replaced for each trial to ensure a smooth interface between the MRF and the plates.

The peak adhesive force normalized by area into a stress observed on a variety of surfaces is plotted as a function of fluid thickness in Figure 2.

C. Failure Time

In order to investigate the holding time of MRF adhesive, pseudo-creep tests were performed. Using the results shown in Figure 2, a failure stress of 18 kPa was determined to be an average failure stress across a wide range of fluid thicknesses. This stress level was chosen as the maximum acceptable load for the robot described in Section V. The testing machine subjected samples prepared as detailed in Section III-A to a fraction of this tensile stress level and recorded the displacement over time until failure or 300 seconds (the maximum allowed test time).

A plot of the time to fail of the MRF as a function of load and fluid thickness is shown in Figure 3.

IV. RESULTS

A. Failure Stress

The results of the probe-tack experiment are shown in Figure 2. The adhesive force from the unactivated fluid increased by at least an order of magnitude when the magnet was introduced. The existence of any normal force in the off-state was due to the small yield stress σ_{y0} in Equation 2 and the non-zero strain rate.

In the range of 150 μm to 1000 μm fluid thickness, no clear relationship existed between the thickness and the failure force, although Equation 3 would suggest an inverse relationship between thickness and force.

In contrast to Ewoldt *et al.*'s observations of slip-stick behavior during adhesive failure in [16], the MRF in these experiments behaved like a brittle material. Ewoldt and the derived model assumed cohesive failure; that is, the MRF yields and deforms to relieve the applied strain. In this study, however, the primary observed failure mechanism was interfacial; the MRF slowly detached from the surface until failing in a single brittle event. Photographs from before and after adhesive failure are shown in Figure 4, which depicts the rapid detachment. The force model detailed in Equation 3 dramatically over-predicted the achievable loads, further implying that the observed data resulted from an unmodeled failure mechanism.

Surface roughness had a detrimental effect on adhesive force. The observed results for the MRF on sandpaper showed less than half the adhesion strength as compared to smooth surfaces; however, it should be noted that this a very wide range of surface roughnesses, and the MRF demonstrated adhesion to the complete range. Additional tests (not shown) on smooth aluminum and teflon showed similar failure forces as acrylic.

B. Failure Time

The results of the pseudo-creep tests are shown in Figure 3. Consistent with the brittle behavior observed in Section IV-A, the samples displaced very little until catastrophic failure, as depicted in Figure 4. Higher loads tended to fail more quickly, but increased fluid thickness resulted in an increased hold time. These observations correlated with the trends observed in Figure 2, but again disagreed with the cohesive failure-based model given in Section II. .

V. ROBOTIC DESIGN

A. Design Concepts

Initial design concepts focused on small, low-profile robots. From Figure 2 it was determined that 18 kPa was a reasonable average value for the failure stress of MRF activated by a field

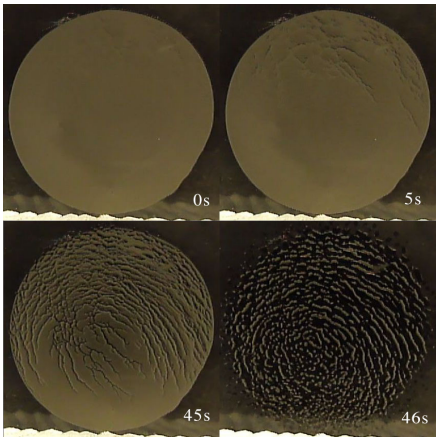

Fig. 4. Four images taken from underneath the transparent bottom plate during a probe-tack test. The MRF is 24 mm in diameter and 160 μm thick, and is activated by a uniform normal flux of 0.2 T.

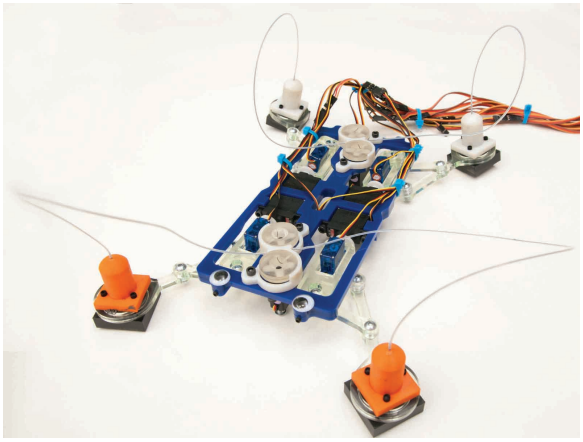

Fig. 5. The magnetorheological adhesion climbing robot.

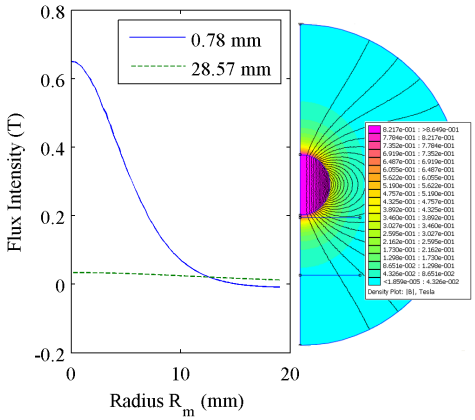

Fig. 6. The magnetic flux produced by a 19 mm spherical neodymium magnet normal to planes located 0.78 mm and 28.57 mm away from one pole. The right plot shows the flux field, where warmer colors represent higher fields and flux lines are drawn in black.

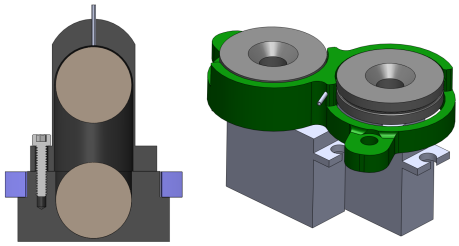

Fig. 7. The permanent magnet actuation assembly. The left image is a cross-sectional view of the robot foot, showing the two extreme positions of the magnet. The actuator cable enters through the tube at the top while the flexible sheath is press-fit around it. The right image shows the cable actuation assembly; the wire enters the tube shown in the middle and wraps up to halfway around the spool. The front and back spool pairs are combined for efficiency.

of 0.2 T; a safety factor of slightly less than 2 reduced the expected working stress to 10 kPa.

From this value, a robot with an overall maximum footprint of approximately 30 cm by 30 cm with a total mass less than 1 kg was chosen as a reasonable compromise between weight constraints and magnetic field production. Ultimately a four-legged walking design was chosen. A treaded tank-style design was also considered but rejected due to the problem of sufficiently tensioning the tread to prevent separation from the main body during inverted driving.

B. Magnets

Actuated permanent magnets were chosen as the magnetic field sources for the robot. Electromagnets and electro-permanent magnets [18] were desirable choices due to their solid-state construction but were rejected due to high power requirements. The data sheet for the MRF [17] specifies that the maximum yield stress is produced by an applied magnetic flux of 0.6 - 0.9 T; an air-core electromagnet producing this flux would require a current density of 150 A/mm for the entire duration of the adhesion. Electro-permanent magnets required similar currents, albeit for much shorter time scales. This power requirement was deemed unacceptable for a mobile robot.

19 mm diameter grade 42 spherical neodymium permanent magnets were used. Cylindrical magnets would have been preferable to spherical magnets, as their geometry would allow a closer interaction between the magnet and the MRF; however, the chosen spherical magnets were found to be sufficient replacements. As shown in Figure 6, these magnets produced a flux field greater than 0.2 T over a 8 mm radius circle 0.78 mm away from one pole, with a weaker field remaining out to a 15 mm radius. This 8 mm circle enclosed an area of 200 mm^2; assuming the additionally activated fluid in the 15 mm circle made a small contribution, four such magnets were sufficient to bear the kilogram load.

C. Magnetic Actuation

The robot's feet were designed in two halves made from of machined Delrin and 3D-printed VeroWhite resin, held together by nylon bolts. The foot sole had dimensions of 38 mm x 38 mm to fully exploit the maximally active circle of the magnet. Each foot had a pill-shaped cavity through which

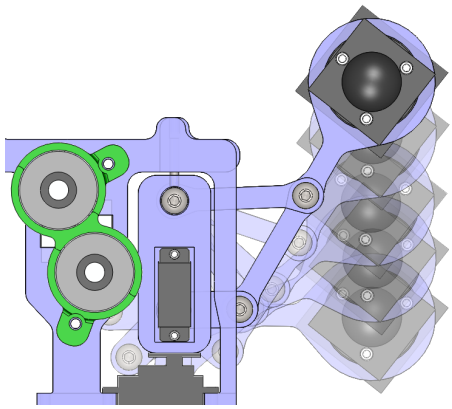

Fig. 8. The path of one foot during a stepping action. The step length is approximately 10 cm.

the spherical magnets could translate. In the "on" state, the magnet settled into a semi-circular cavity machined to be 0.78 mm away from the sole; in the "off" state, the magnet was pulled 28.57 mm away from the sole, as shown in Figure 7. The magnetic fields along the bottom surface of the foot for both cases (assuming the magnet was oriented with with one pole toward the MRF) are shown in Figure 6.

The magnet was actuated using a Bowden cable; a length of 24 AWG spring steel wire connected to one pole of the magnet and ran to a remote actuator located on the body of the robot. The wire traveled within a flexible but inextensible sheath that joined the foot and the body. On the body, the wire connected to a cylindrical horn on a servomotor; this horn was surrounded by a co-axial cylindrical wire guide, both of which were constructed via 3D-printing. When the servo turned the magnet "off," the wire spooled around the cylinder; when the magnet was turned "on," the wire pressed against the guide and fed back into the sheath, driving the magnet toward the sole of the foot.

This actuation scheme eliminated the need for a servo to be located on the foot, despite the relative motion between the foot and the body throughout the stepping motion. The gage of the wire was sufficient to support the magnet's weight, ensuring that it would not buckle even if the robot were on the ceiling.

D. Movement

The leg was composed of a laser cut 6 mm acrylic arranged in a Hoekens-type four bar mechanism driven by a single servo mounted in the ground link. This linkage was tuned such that the foot traced a straight line parallel to the main axis of the robot, as shown in Figure 8. The two halves of the foot assembled through a 35 mm round hole at the end of the leg. This connection secured the foot to the leg while leaving the rotation of the foot unconstrained. If instead a rigid connection were used between the two, the motion of the leg would cause the foot to twist in place and potentially break the adhesive connection to the surface as the robot drew its body forward.

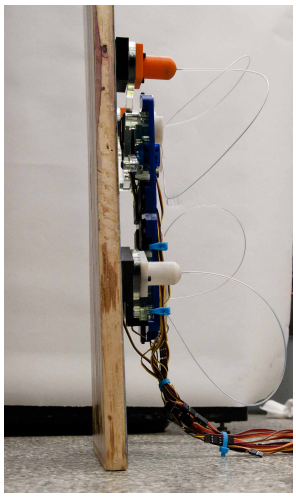

Fig. 9. The robot adhering to a vertical board covered with 150 grit sanding cloth. The MRF sustained a shear of approximately 7.6 kPa; without the MRF, the robot slid at an angle of approximately 45°, or a stress of 0.96 kPa.

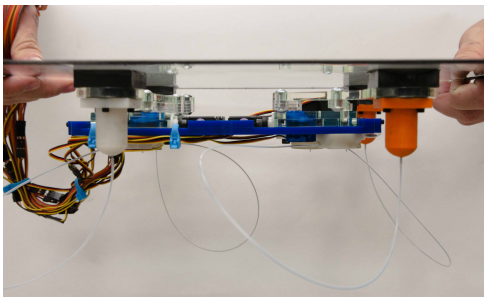

Fig. 10. The robot hanging completely inverted beneath a glass sheet. The adhesion stress is approximately 7.6 kPa.

Each leg was mounted between a servo and a pin in a loose-fit hole, such that the entire leg could be pivoted like the wing of a bird. The body was made from laser cut 6 mm acrylic, similar to the legs. Each leg had three servos which actuated the stepping, wing motion, and magnet, for a total of twelve across the entire robot. At full leg extension the robot had a footprint of 320 mm x 230 mm and had a mass of 790 grams.

E. Testing

Mechanical problems prevented the robot from walking in time for this paper; however, the magnetic actuation was shown to be effective at activating and deactivating the MRF adhesive effect. The robot was able to engage and disengage from the target surface by actuating the wing and magnet movements.

Figures 9 and 10 depict the robot adhering to a vertical board covered with 150 grit waterproof sanding cloth and an inverted glass sheet. Assuming the 8 mm radius circle observed in Section V-B is the adhesive area, the adhesive stress in both cases is 7.6 kPa.

Four approximately 1 cm^3 drops of MRF were placed on the sanding cloth and glass, arranged appropriately for the robot feet. The robot was placed into position with deactivated

magnets; once in position, the magnets were activated. After the sanding cloth board was slowly rotated from horizontal to vertical, the robot remained adhered to the vertical surface for several minutes. The robot was observed to slide on the glass under very light shear loads, so it was gently held in place while it and the glass were overturned together. It adhered to the underside of the glass, unassisted, for approximately 30 seconds before failure.

VI. CONCLUSIONS AND FUTURE WORKS

A. Conclusions

Experiments measuring the tensile failure force and time to failure of strongly activated magnetorheological fluid between two parallel plates. The results were compared to existing fluid models and found to be an order of magnitude lower, indicating the need for a model that incorporates adhesive failure. Surface roughness was shown to have a detrimental effect upon adhesive force.

These results drove the design of a robot based on this novel form of magnetorheological adhesion. By actuating permanent magnets, the robot was able to exploit two distinct fluidic behaviors to adhere to surfaces of varying roughness and orientation, including complete inversion. Adhesion stresses of approximately 7.6 kPa were achieved in both shear and direct adhesion.

B. Future Works

Further basic investigation into the effects of roughness, material properties, surface misalignment, and fouled surfaces is on adhesive force is necessary. Building upon this work, a more comprehensive theoretical model incorporating the limiting failure mechanism observed in this paper and resolving the discrepancy between the slip-stick and brittle failure models is necessary.

Future work on the robot will focus on expanding the range of traversable surfaces and incorporating an on-board fluid reservoir for autonomous behavior. Of particular interest was the need to preload the feet; in order to adequately spread the MRF into a thin layer covering the entirety of the foot, it was necessary to move the feet back and forth under load. The weight of the robot was sufficient while on a horizontal surface, but on vertical or inverted surfaces this additional force manifests as another load on the remaining feet. The disturbance on the other feet could be reduced by adding more feet or utilizing more wettable surfaces for more efficient spreading.

VII. ACKNOWLEDGMENTS

The authors gratefully acknowledge the contributions of Professors Anette Hosoi and Gareth McKinley, as well as Nadia Cheng, Ahmed Helal, and Maria Telleria for their assistance in conducting these experiments and designing the robot.

REFERENCES

[1] K. Daltorio, A. Horchler, S. Gorb, R. Ritzmann, and R. Quinn, "A small wall-walking robot with compliant, adhesive feet," in *2005 IEEE/RSJ International Conference on Intelligent Robots and Systems, Vols 1-4*, IEEE; Robot Soc Japan. 345 E 47TH ST, NEW YORK, NY 10017 USA: IEEE, 2005, Article, pp. 4018–4023, IEEE/RSJ International Conference on Intelligent Robots and Systems, Edmonton, CANADA, AUG 02-06, 2005.

[2] A. T. Asbeck, S. Kim, M. R. Cutkosky, W. R. Provancher, and M. Lanzetta, "Scaling hard vertical surfaces with compliant microspine arrays," *INTERNATIONAL JOURNAL OF ROBOTICS RESEARCH*, vol. 25, no. 12, pp. 1165–1179, DEC 2006, Conference on Robotics - Science and Systems, Cambridge, MA, JUN, 2005.

[3] A. Saunders, D. I. Goldman, R. J. Full, and M. Buehler, "The RiSE climbing robot: Body and leg design - art. no. 623017," in *Unmanned Systems Technology VIII, Pts 1 and 2*, ser. PROCEEDINGS OF THE SOCIETY OF PHOTO-OPTICAL INSTRUMENTATION ENGINEERS (SPIE), Gerhart, GR and Shoemaker, CM and Gage, DW, Ed., vol. 6230, no. Part 1-2, SPIE. SPIE-INT SOC OPTICAL ENGINEERING, 2006, Article, p. 23017, Conference on Unmanned Systems Technology VIII, Kissimmee, FL, APR 17-20, 2006.

[4] K. Autumn, A. Dittmore, D. Santos, M. Spenko, and M. Cutkosky, "Frictional adhesion: a new angle on gecko attachment," *JOURNAL OF EXPERIMENTAL BIOLOGY*, vol. 209, no. 18, pp. 3569–3579, SEP 15 2006.

[5] M. Lanzetta and M. Cutkosky, "Shape deposition manufacturing of biologically inspired hierarchical microstructures," *CIRP Annals - Manufacturing Technology*, vol. 57, no. 1, pp. 231–234, 2008. [Online]. Available: http://linkinghub.elsevier.com/retrieve/pii/S0007850608000541

[6] B. Yurdumakan, N. Raravikar, P. Ajayan, and A. Dhinojwala, "Synthetic gecko foot-hairs from multiwalled carbon nanotubes," *CHEMICAL COMMUNICATIONS*, no. 30, pp. 3799–3801, 2005.

[7] Y. Zhao, T. Tong, L. Delzeit, A. Kashani, M. Meyyappan, and A. Majumdar, "Interfacial energy and strength of multiwalled-carbon-nanotube-based dry adhesive," *JOURNAL OF VACUUM SCIENCE & TECHNOLOGY B*, vol. 24, no. 1, pp. 331–335, JAN-FEB 2006.

[8] M. Sitti and R. Fearing, "Synthetic gecko foot-hair micro/nano-structures as dry adhesives," *JOURNAL OF ADHESION SCIENCE AND TECHNOLOGY*, vol. 17, no. 8, pp. 1055–1073, 2003.

[9] M. Northen and K. Turner, "A batch fabricated biomimetic dry adhesive," *NANOTECHNOLOGY*, vol. 16, no. 8, pp. 1159–1166, AUG 2005.

[10] H. Gao, X. Wang, H. Yao, S. Gorb, and E. Arzt, "Mechanics of hierarchical adhesion structures of geckos," *MECHANICS OF MATERIALS*, vol. 37, no. 2-3, pp. 275–285, FEB-MAR 2005, Workshop on new Directions in Mechanics, Warrenton, VA, SEP 07-10, 2003 .

[11] S. Kim and M. Sitti, "Biologically inspired polymer microfibers with spatulate tips as repeatable fibrillar adhesives," *APPLIED PHYSICS LETTERS*, vol. 89, no. 26, DEC 25 2006.

[12] C. Balaguer, A. Gimenez, J. Pastor, V. Padron, and C. Abderrahim, "A climbing autonomous robot for inspection applications in 3D complex environments," *ROBOTICA*, vol. 18, no. Part 3, pp. 287–297, MAY-JUN 2000.

[13] Z. Xu and P. Ma, "A wall-climbing robot for labelling scale of oil tank's volume," *ROBOTICA*, vol. 20, no. Part 2, pp. 209–212, MAR-APR 2002.

[14] K. Yatsuzuka, J. Toukairin, and K. Asano, "Electrostatic chuck with a thin ceramic insulation layer for wafer holding," in *CONFERENCE RECORD OF THE 2001 IEEE INDUSTRY APPLICATIONS CONFERENCE, VOLS 1-4*, ser. IEEE Industry Applications Society Annual Meeting, IEEE; Ind Appl Soc. IEEE, 2001, Article, pp. 399–403.

[15] G. Monkman, "Electroadhesive microgrippers," *INDUSTRIAL ROBOT-AN INTERNATIONAL JOURNAL*, vol. 30, no. 4, pp. 326–330, 2003.

[16] R. Ewoldt, P. Tourkine, and G. McKinley, "Controllable adhesion using field-activated fluids," *Physics of Fluids*, vol. 23, no. 7, 2011. [Online]. Available: http://link.aip.org/link/?PHFLE6/23/073104/1

[17] "MRF-132DF Magneto-Rheological Fluid," *LORD Technical Data*, pp. 1–2, Jul. 2008. [Online]. Available: http://www.lordfulfillment.com/upload/DS7015.pdf

[18] A. N. Knaian, "Electropermanent Magnetic Connectors and Actuators: Devices and Their Application in Programmable Matter," Ph.D. dissertation, Massachusetts Institute of Technology, Cambridge, MA, May 2010.